Brazilian Journal of Geophysics 42 (2024), 3, 1-23
Brazilian Geophysical Society
ISSN 2764-8044
DOI: 10.22564/brjg.v42i3.2324

# ENHANCEMENT OF DETECTION CAPABILITIES AT THE BRASÍLIA INFRASOUND STATION: BRAZIL'S CONTRIBUTION TO THE INTERNATIONAL MONITORING SYSTEM (IMS) OF THE COMPREHENSIVE NUCLEAR-TEST-BAN TREATY (CTBT)

Darlan P. Fontenele and Lucas V. Barros

Universidade de Brasília – UnB, Seismological Observatory, Brasília, DF, Brazil

Corresponding author email: dpfontenele@gmail.com

**ABSTRACT.** The Brasília Infrasound Station (designated IS09), the only infrasound station in Brazil, is operated by the Seismological Observatory of the University of Brasilia in collaboration with the Preparatory Commission for the Comprehensive Nuclear-Test-Ban Treaty Organization (PrepCom/CTBTO). Located in the Brasília National Park, the station comprises a four-element array, forming a triangle approximately 2 km aperture with a central element. The inter-distances and the number of array elements are limiting the effectiveness in detecting local and regional events (distances < 1000 km). To overcome this restriction, PrepCom/CTBTO is modernizing the global infrasound network of the International Monitoring System. This initiative aims to standardize and enhance sensitivity by increasing the array's elements from four to eight (or nine). In this study, simulations utilizing the DTK-GPMCC computational tool, involving the addition of five elements to the former IS09, reveal a significant enhancement in the station's performance. Shorter inter-distances between the new elements (ranging from 150 to 900 meters) lead to increased detections and reduced spatial aliasing effects for frequencies above 1 Hz. Analysis of the array response function demonstrated that the gain achieved with the new array is fivefold compared to the previous configuration, besides expanding the frequency bandwidth, thereby allowing the detection of local and regional events. This work also includes the development of a mechanical filter that reduced the amplitude response noise by a factor of 10 between 0.6 and 10 Hz in the employed temporary stations.

**Keywords:** IS09 station; PrepCom/CTBTO; array element inter-distances; spatial aliasing in infrasound arrays; infrasound array enhancement; array sensitivity and frequency bandwidth; environmental noise mitigation in infrasound detection

## INTRODUCTION

Sensor arrays characterize wavefront arrivals in several application areas, such as seismology, astronomy, geodesy, etc. The spatial resolution and sensitivity of an array are determined by factors such as the sensors number, spacing, and the respective distribution of them (Bishop et al., 2020; Ruigrok et al., 2017). According to the Nyquist sampling theorem, a discrete sampling of the wavefront representation in time and space imposes some restrictions on the width of the wavefront frequency band and respective wavelengths that the array can resolve satisfactorily. For spatial sampling to unambiguously capture a given wavelength λ, the spacing between array elements, denoted as "d" in the ray's direction, must be smaller than λ/2. Furthermore, the wavenumber k ($k= 2\pi/\lambda$) resolution requires at least the array aperture "D" equal to λ. Expressed as mathematical conditions, these requirements can be represented as $2d < \lambda < D$ (Havskov and Alguacil, 2004).

The detection capability of infrasound stations formed by four-element arrays is limited due to spatial aliasing effects, characterized by erroneous frequency identification, resulting in distortion or error in the information contained in the signal (Campus and Christie, 2010; Green and Bowers, 2010; Green, 2015). Spatial aliasing occurs when the spacing between sensors (inter-distances) is too large relative to the incident signal's spatial frequency (wavenumbers). In turn, the sensor array cannot distinguish the high-frequency spatial variations present in the wavefront, leading to misrepresented information and potential signal distortion.

The Brasília Infrasound Station, designated IS09 (Barros and Fontenele, 2002), one of the sixty global network stations of the International Monitoring System (IMS), is operated by the Seismological Observatory of the University of Brasília (SIS-UnB) in collaboration with the Preparatory Commission for the Comprehensive Nuclear-Test-Ban Treaty Organization (PrepCom/CTBTO), clearly illustrates this limitation. The four elements of the IS09 array are distributed at the vertices of a triangle, with one element close to the center. The maximum spacing between elements is about 2 km, and the minimum is about 1 km. They are in a savannah area with typical vegetation of this biome within the Brasília National Park (PNB), an area of permanent environmental preservation (Fig. 1), as described by Barros and Fontenele (2002). The low tree density typical of this biome favors wind incidence, leading to increased noise levels. According to Bowman et al., 2005, this noise can mask potential detections depending on its intensity. To address these challenges, the Provisional Technical Secretariat (PTS) of PrepCom/CTBTO is modernizing the IMS infrasound stations to standardize and enhance their performance. This ongoing initiative aims to overcome the limitations of four-element arrays, ultimately improving the quality and accuracy of data collected by the network's infrasound stations.

According to the requirements of the Comprehensive Nuclear-Test-Ban Treaty (CTBT) verification system, through the IMS, the infrasound frequency band for detecting nuclear explosions must be between 0.02 to 4 Hz (Dahlman et al., 2011). Currently, the frequency range detectable by station IS09 is below 1 Hz, therefore, does not have the bandwidth to detect signals from local and regional events (distances < 1000 km), corresponding to the higher frequencies specified by the

CTBT verification system. Thus, there is a pressing need to modernize the station by increasing the number of elements with shorter inter-distances. This expansion will enable the station to detect events in a broader range, complying with the requirements established in the CTBT, and enabling the detection of events originating from sources other than those currently detected.

Initially, the infrasound wave is captured through an efficient mechanical filter, using a device composed of four rosettes in each element of the IS09 connected to the microbarometer. These structures consist of metal tubes linked to a central core resembling a rosette and aim to eliminate incoherent signals generated by the wind. In doing so, preserves only the coherent signals from infrasonic events, as described by Alcoverro (1998), Alcoverro and Le Pichon (2005), and Walker and Hedlin, 2010. This mechanical filter comprises the Wind Noise Reduction System (WNRS).

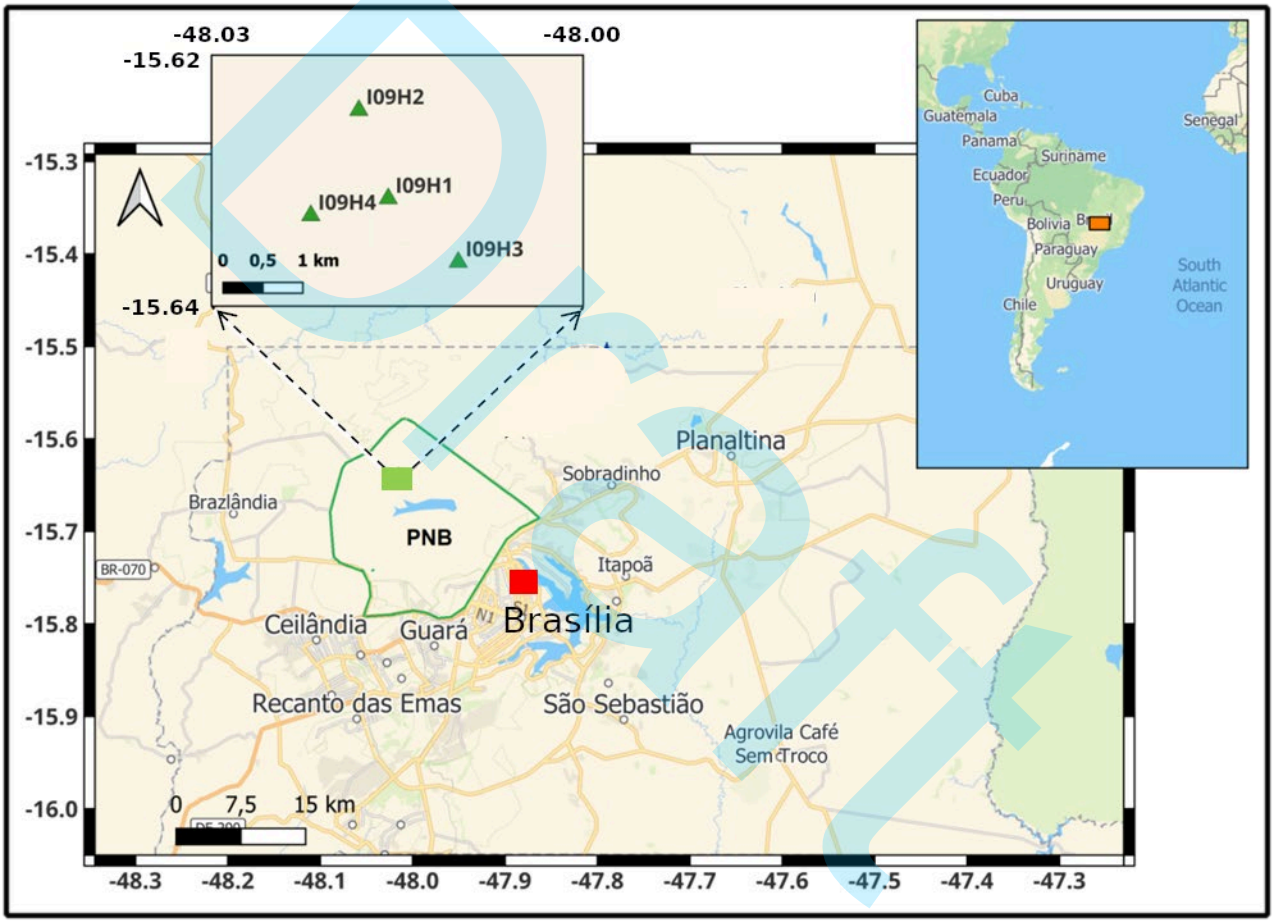


**Figure 1 –** Location map of the four elements of the IS09 station (green triangles) inside the Brasília National Park (PNB). The red square indicates the location of the Central Recording Facility (CRF), situated at the Seismological Observatory of the University of Brasília (SIS-UnB), where data are received, recorded, analyzed, and retransmitted to the International Data Center (IDC), Vienna, Austria (Barros et al., 2020).

In this work, modifications are made to the IS09 array, with the addition of five new elements, aiming to increase the station's gain as well as extend the frequency band to satisfy the requirements for detecting local and regional events.

## METHOD

The IMS Operational Manual defines general requirements for infrasound stations (Conference on Disarmament, 1995; CTBTO, 1997), including the minimum number of array elements (four), array geometry (triangle with a component at the center), and array aperture (1 to 3 km, with a recommended spacing of 3 km). These minimum requirements can be adjusted for noisy locations or when an increase in station detection capability is necessary (CTBTO, 2009).

Following the initial installations of IMS infrasound stations, concerns emerged regarding the limited capacity of stations with four-element arrays. Thus, a recommendation was made to increase the number to up to eight, aiming for a balance between signal detection and costs. Most subsequent stations were built with a minimum of eight elements, and some existing ones were upgraded accordingly. The current number of elements in arrays varies from 4 to 15, with most stations having 4 or 8 elements (CTBTO, 2001).

The 2003 Expert Meeting on IMS array element distribution (CTBTO, 2003) emphasized the importance of adapting array geometry to local conditions and avoiding symmetries, meaning choosing locations with different inter-element spacings. However, these recommendations were not always followed in new IMS stations. The design of IMS infrasound arrays involves a balance between detection and accuracy in estimating wave parameters. This balance is primarily affected by the coherence loss of infrasound signals with distance and background noise levels at the station location. Installing array elements in locations with low background noise is crucial, prioritizing practical considerations over the pursuit of a theoretically perfect geometry. Key design criteria include land constraints, noise levels, homogeneous distributions of distance and azimuth, resilience to element loss, and costs (Marty, 2019).

Maintaining signal coherence based on the spacing between array elements and minimizing the spatial aliasing of high-frequency signals will significantly increase the detection capability of a station. Employing arrays with eight or nine elements, featuring optimized designs in infrasound monitoring stations, significantly enhances signal coherence. Additionally, depending on the spacing between elements, the signal frequency range is extended (Christie, 2007).

In this work, we utilized the NDC-in-a-Box software package (version 5.2), distributed by PrepCom/CTBTO to the states' parties of the CTBT, to model multiple arrays of nine infrasound elements. This number of elements corresponds to the addition of five new ones to the existing four at the IS09 station. Detailed results of each array will not be discussed here. Just one out of 50 modeled arrays stood out for its promising ability to mitigate spatial aliasing effects at frequencies above 1 Hertz for an omnidirectional signal receiving. Moreover, this particular array provides the expansion of the frequency band to detect local and regional events, aligning with the objectives of this research.

Within of NDC-in-a-Box package were added functionalities to the Dase ToolKit - Graphical Progressive Multi-Channel Correlation (DTK-GPMCC) program, developed by the Commissariat à l'Energie Atomique – Département Analyze Surveillance Environnement (CEA-DASE, 2016). DTK-GPMCC allows the analysis of infrasonic signals and the extraction of parameters related to the

station (array), including array response and uncertainties associated with the azimuth and speed of infrasonic waves. DTK-GPMCC incorporates a database with information from all IMS infrasound stations regarding geometry, the number of elements, array response, and uncertainties associated with trace velocity and azimuth. The tool also uses the Progressive Multichannel Correlation Method (PMCC), as introduced by Cansi (1995), for data processing in the search for detections. This method utilizes the average degree of estimated signal correlation, a concept presented by Mack and Flint (1971). Signal processing through DTK-GPMCC is carried out by choosing eleven consecutive and simultaneous frequency bands, ranging from 0.07 to 4.0 Hz (close to the IMS frequency band, 0.02 - 4.0 Hz), in windows of adjacent times, covering the entire period of the analyzed signal. The duration of each time window depends inversely on the frequency range. In practice, time windows of 60 seconds are used for the lowest frequencies and 30 seconds for the highest frequencies (Brachet et al., 2010). Consequently, DTK-GPMCC was also employed to evaluate the empirical results of the modeled chosen array using the data generated by the elements from that array installed in the Brasilia National Park (PNB) temporarily, allowing the comparison results between the nine-element array and a four-element subarray, this last one sharing the same sites of the IS09 elements.

We have used the Array Response Function (ARF) equation to calculate the array sensitivity based on the number and distribution (inter-distances) of its elements. The study also explores how the array behaves concerning the wave frequency (wavenumbers) of the plane wavefront, considered as such in this study, incident upon the array elements (Ruigrok et al., 2017). This study developed a code in Obspy (Beyreuther et al., 2010) to implement the ARF as a function of the frequency (f), wave velocity (c), and wavenumber vector (k) kx and ky, according to the following equation:

$$ARF\left(f, c, k_x, k_y\right) = \sum_{i=1}^{N} \sum_{j=1}^{N} e^{j2\pi f\left(\frac{k_x \cdot \Delta x_{il}}{c} + \frac{k_y \cdot \Delta y_{il}}{c}\right)}.$$

where:

summations where i (sensor location i) and l (sensor location l) vary from 1 to N (the number of sensors in the array).

f is the wave frequency (Hz).

c is the wave propagation velocity (m/s).

$k_x$ and $k_y$ are the components of the wave vector (rad/m).

$\Delta x_{il}$ and $\Delta y_{il}$ are the positional differences between sensors i and l in the array.

This equation represents the contribution of each pair of sensors i, l to the Array Response Function, considering the positional differences and the characteristics of the incident wave.

We have utilized the Power Spectral Density (PSD) (Peterson, 1993) to assess the background noise of each element, considering signal amplitudes across various recorded frequencies. This analysis aimed to understand the levels of noise present in the records, taking into account sources such as wind-induced turbulence and anthropogenic factors that could hinder efficient station detection (McNamara and Buland, 2004). The curves representing the new low noise model (NLNM) and the new high noise model (NHNM) are plotted alongside the element records on

the graph. These curves serve as a reference to evaluate the intensity of the background noise for each element, with lower noise indicating a higher signal-to-noise ratio (SNR) for the element.

***Installation of temporary elements in the Brasília National Park (PNB)***

Installing temporary elements in the Brasília National Park (PNB) served to validate and demonstrate the improved response of the theoretical (modeled) array compared to the existing four-element array at the IS09 station. Nine units of equipment, specifically RaspberryShake Company's RSandBoom model, were utilized for this purpose. These units comprised a barographic sensor (differential pressure transducer with a flat band frequency response ranging from 1 to 44 Hz) connected to a digitizing board. This board was coupled to a Raspberry Pi 3, model B computer, integrated into a compact IP67 plastic box measuring 160x90x90 mm. The choice of this equipment was based on its affordability, quick delivery, and technical characteristics that aligned with the requirements of the experiments conducted in this study, including low energy consumption (less than 5 Watts), acceptable internal noise, and an appropriate frequency band response (RaspberryShake Specifications, 2022). These nine elements were operational in the PNB for 40 days (Fig. 2). Among them, four elements — R7279, R6CF7, R6E11, and R6DF9 — shared locations with the IS09 station (I09H1, I09H2, I09H3, and I09H4, respectively), operating jointly. This configuration allowed for comparisons related to the number of detections obtained from the array (nine-element using RS&Boom) and subarray (four-element using RS&Boom and also using IMS equipment).

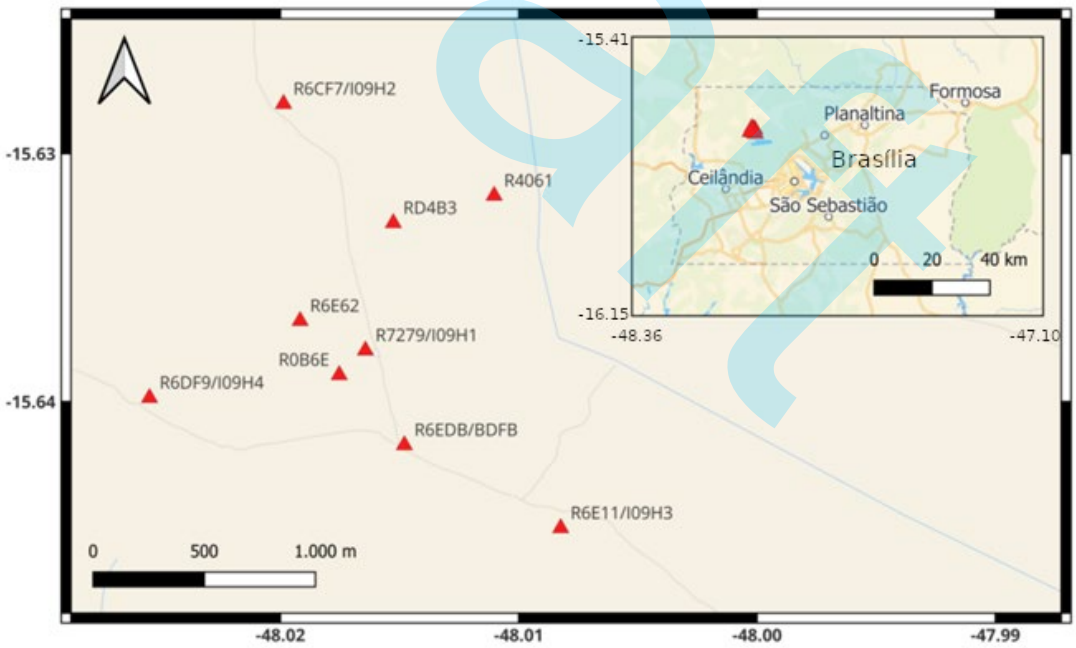


**Figure 2 –** Temporary elements installed in the Brasília National Park (red triangles). The elements locations were selected for the optimization of the array response, accounting for estimated speed and azimuth uncertainties, and resolving spatial aliasing issues through extensive modeling. Double codes indicate elements sharing IS09 station sites.

***Design of the mechanical filter optimized to temporary elements***

A mechanical filter was developed in this study and integrated into the temporary elements using RS&Boom equipment to mitigate wind-induced noise, which affect the detections (Hedlin and Raspet, 2003; Bass and Shields, 2004). The filter comprises polyurethane foam (sponge), measuring approximately 10 x 10 x 10 cm, covered by a layer of crushed stone mesh number 1, with a grain size of around 19 mm. A plastic tube, 1/4" in diameter and 1 meter long, is inserted into the center of the foam, connecting to the inlet port of the RS&Boom barographic sensor (Fig. 3). Figures 4 and 5 provide the practical application of this filter in the temporary elements.

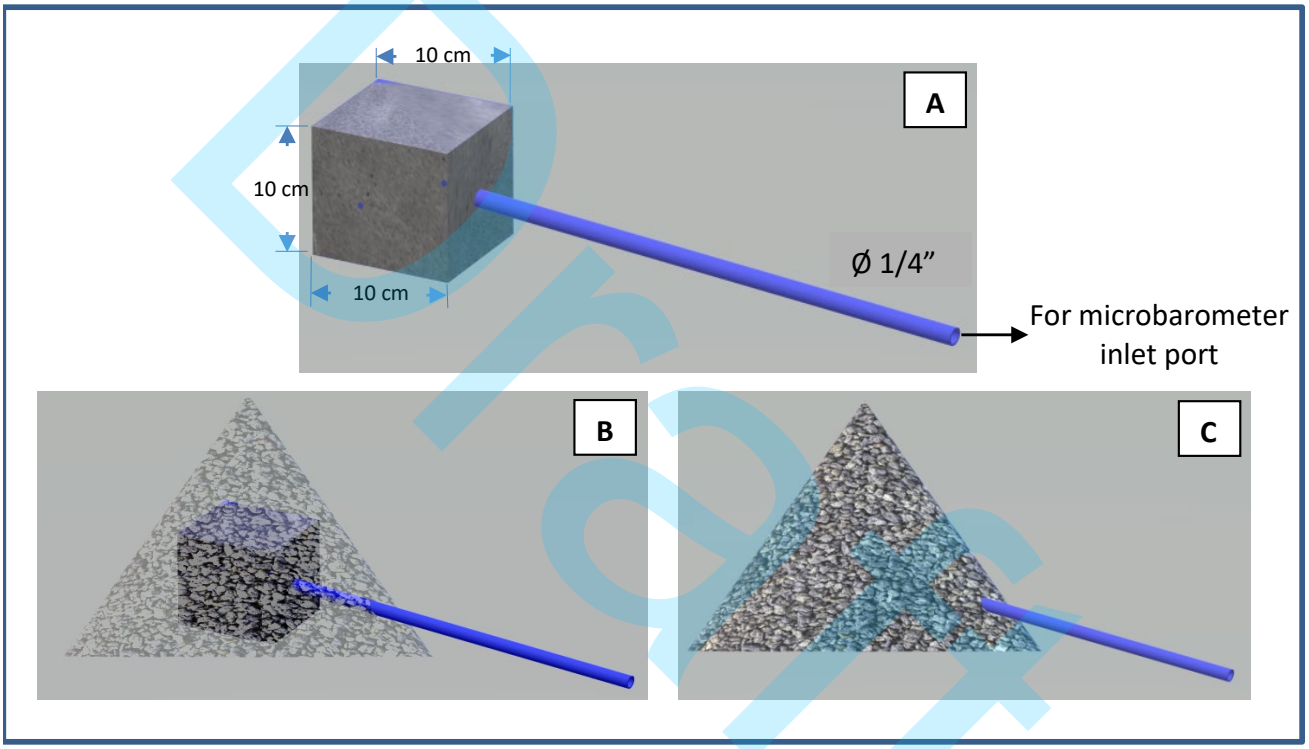


**Figure 3 –** Filter developed to reduce wind noise: **A)** Polyurethane foam with an inserted plastic tube; **B, C)** Layer of gravel covering the foam. The plastic tube connects to the barographic sensor's inlet port (not shown in the figure).

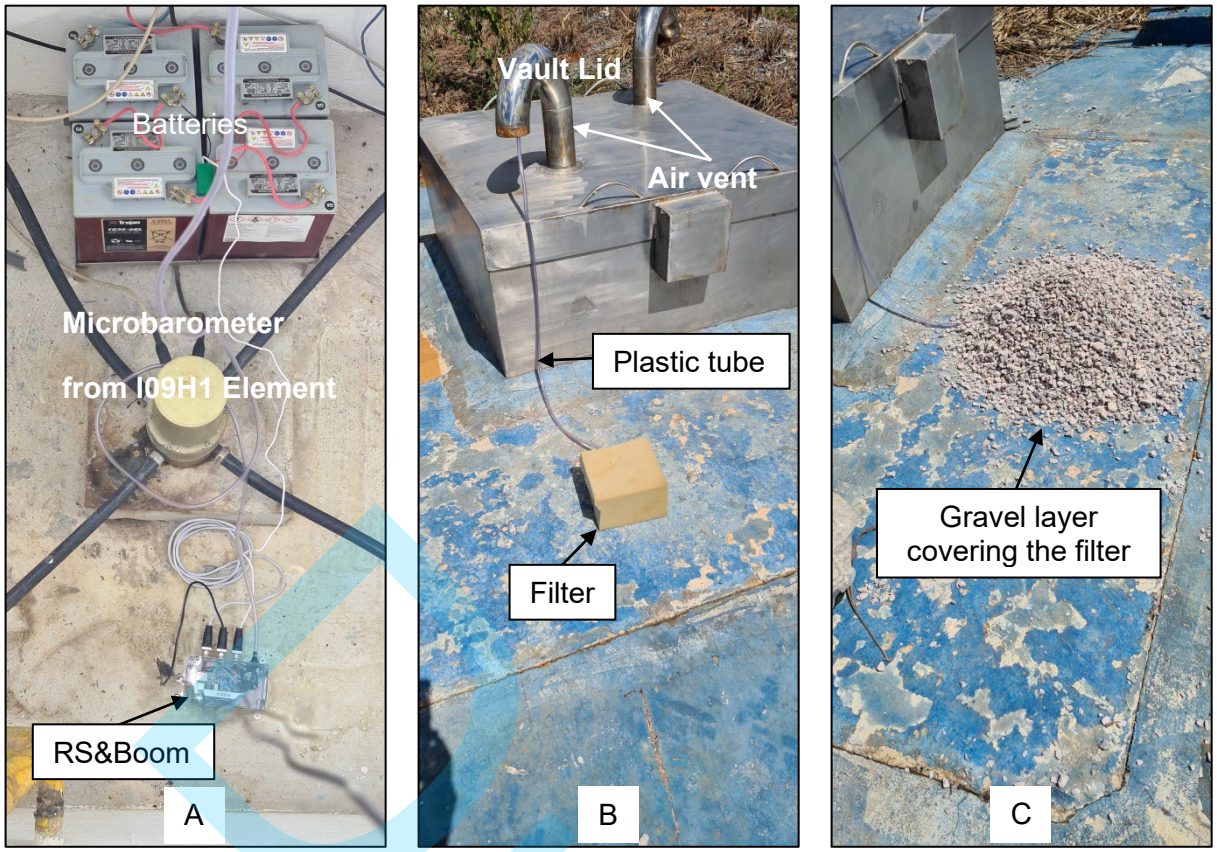


**Figure 4 –** Equipment sharing the I09H1 element site: A) RS&Boom inside the vault; B) View of the filter connected to the RS&Boom through the plastic tube; C) Filter covered by a layer of gravel.


**Figure 5 –** Typical installation of one of the temporary elements: Left – RS&Boom connected to the battery and filter; Right – Protective box for the equipment, a layer of gravel covering the filter, and a solar panel.

## RESULTS

### *Mechanical filter adopted in temporary elements*

A comprehensive evaluation of the filter's efficacy was conducted using two of the nine available equipment units (R7279 and R6CF7). The test involved a three-day phase for each equipment configuration, installed in the same place and during the same periods. In the first phase, R7279 operated with the filter, while R6CF7 operated without it. In the second phase, both equipment units operated without the filter.

The comparative results are illustrated in Figures 6 and 7, revealing the filter's impact. The graph in Fig. 6 shows the difference in the curves within the 0.6 to 10 Hz range, demonstrating a reduction in amplitude response noise by a factor of 10. The curve corresponding to the equipment employing the filter exhibits a lower noise level. In Fig. 7, both equipment units have identical responses from 0.1 Hz onward, meaning no equipment interference was observed in the tests. Some amplitude peaks are also noticeable after 15 Hz, as indicated in Figures 6 and 7. These peaks may be inherent to the equipment's behavior; however, they do not pose a concern as they primarily occur outside the frequency range of the signals of interest in this study. It is important to note that the equipment's frequency range exceeds that of the NHNM and NLNM curves in the graph due to the equipment's response capability extending up to 44 Hz.

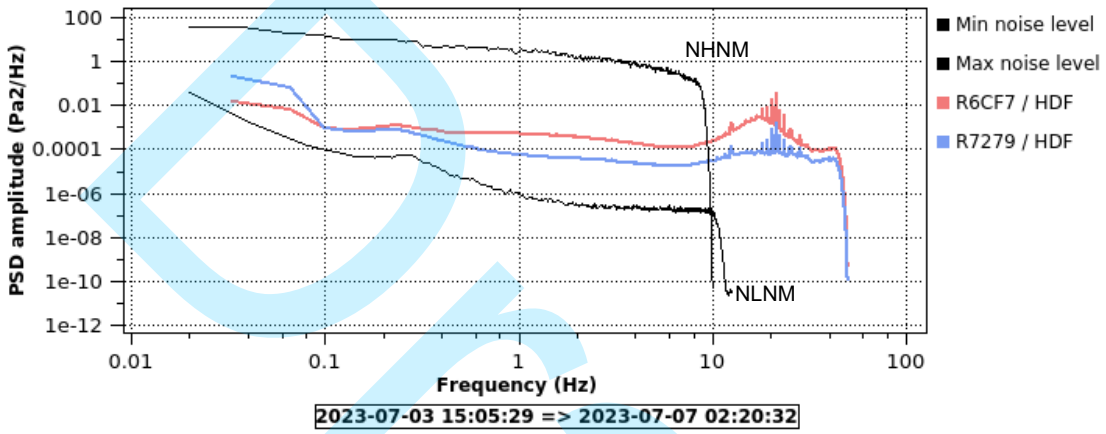


**Figure 6 –** Result of the first phase of the filter test. Equipment R7279 (blue line) is using the filter, and equipment R6CF7 (red line) is without the filter. A reduction, by a factor of 10 between 0.6 and 10 Hz, is observed in the amplitude response curve of the equipment that used the filter.

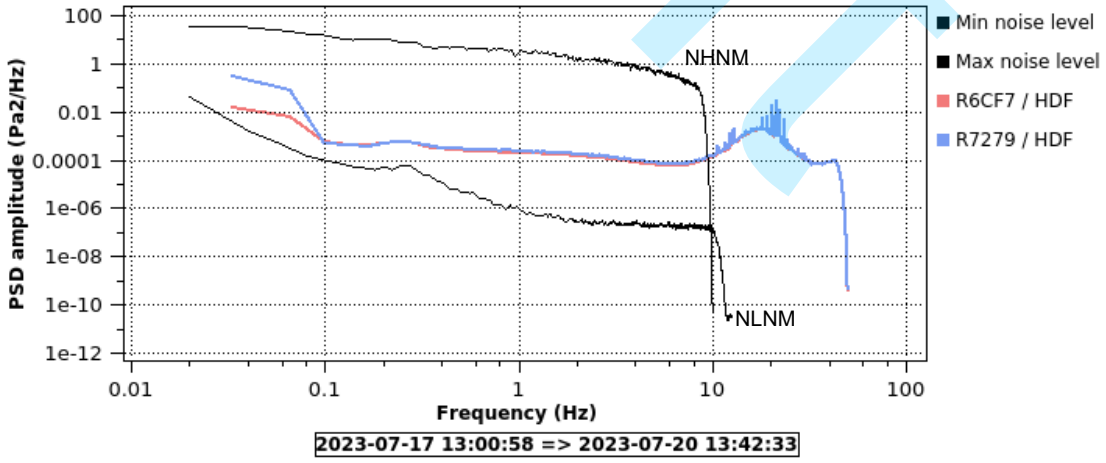


**Figure 7 –** Result of the second phase of the filter test. Both equipment units, R7279 (blue line) and R6CF7 (red line) are depicted without the filter. A precise match in the curves is observed from 0.1 Hz onward, underscoring identical responses in this frequency range for the two devices.

### *Arrays Responses*

Figures 8 to 11 present the responses of the IS09 station array and the proposed nine-element array. These illustrations show the uncertainties associated with the array geometry and element number, the sensitivity of the arrays concerning the wave frequency (wavenumbers) of the plane wavefront incident upon the array elements, and the array behavior based on element distribution. Figures 9 and 11 depict the Array Response Function (ARF) of the four-element and 9-element arrays. Notably, the four-element array exhibits a challenge from 4 Hz onwards (effectively, for frequencies greater than 1 Hz, though not shown in the figures), marked by the emergence of side lobes with significant energy (artifacts). This phenomenon represents a spatial aliasing issue. In contrast, this problem is not observed for the 9-element array. The absence of side lobes in the 9-element array, or when they happen with small energies, indicates improved performance, highlighting the effectiveness of the proposed array configuration in mitigating spatial aliasing, besides the array sensitivity gain.

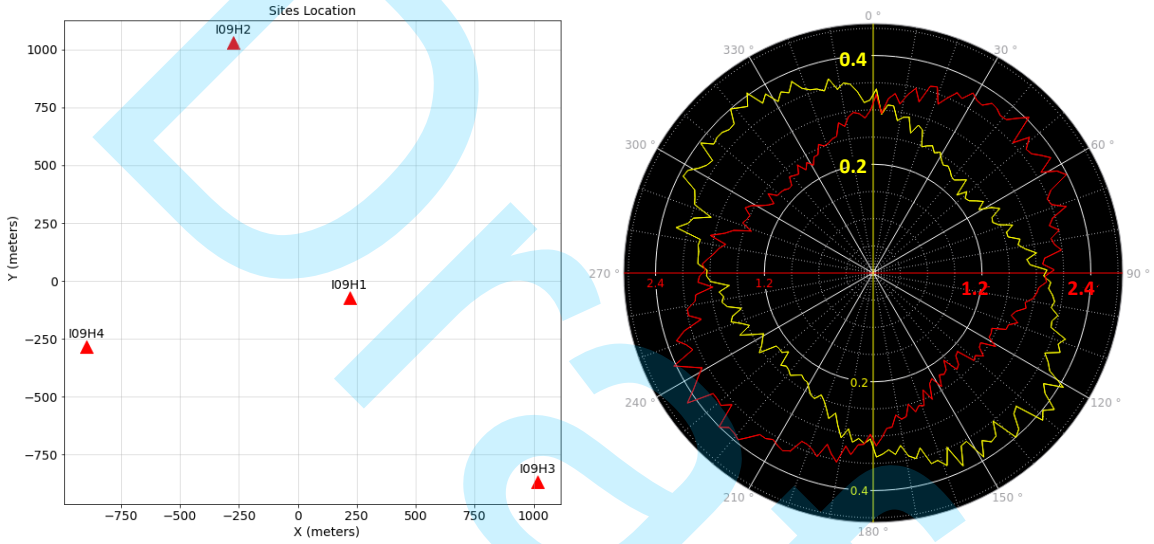


**Figure 8 –** On the left, the four-element array of IS09 station and, on the right, the respective polar graph of the estimated signal speed errors (red line – m/s) and azimuth (yellow line – degrees) for plane wavefronts propagating at 340 m/s. The signal sampling rate is 20 sps.

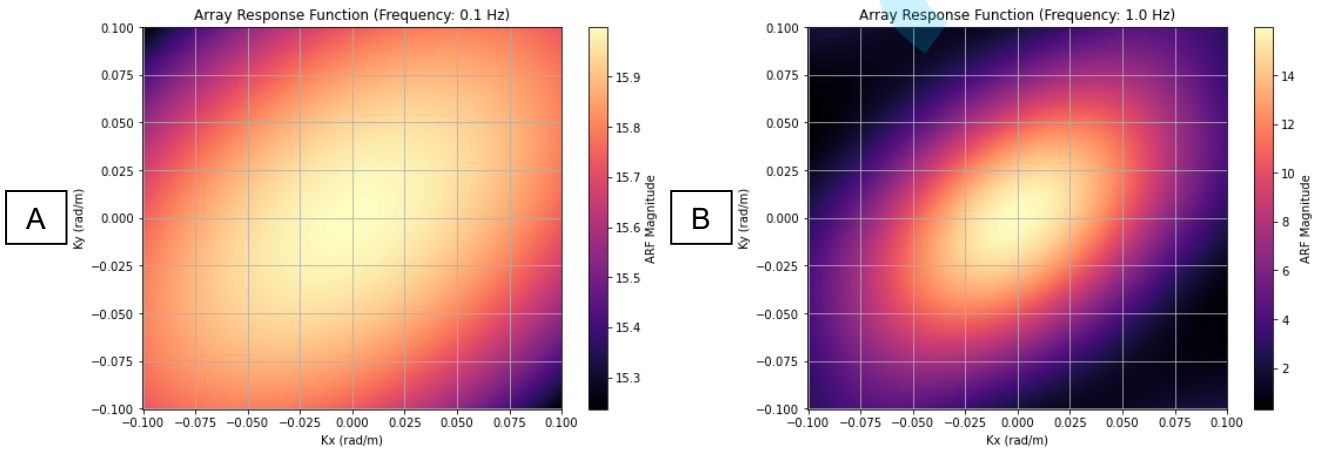

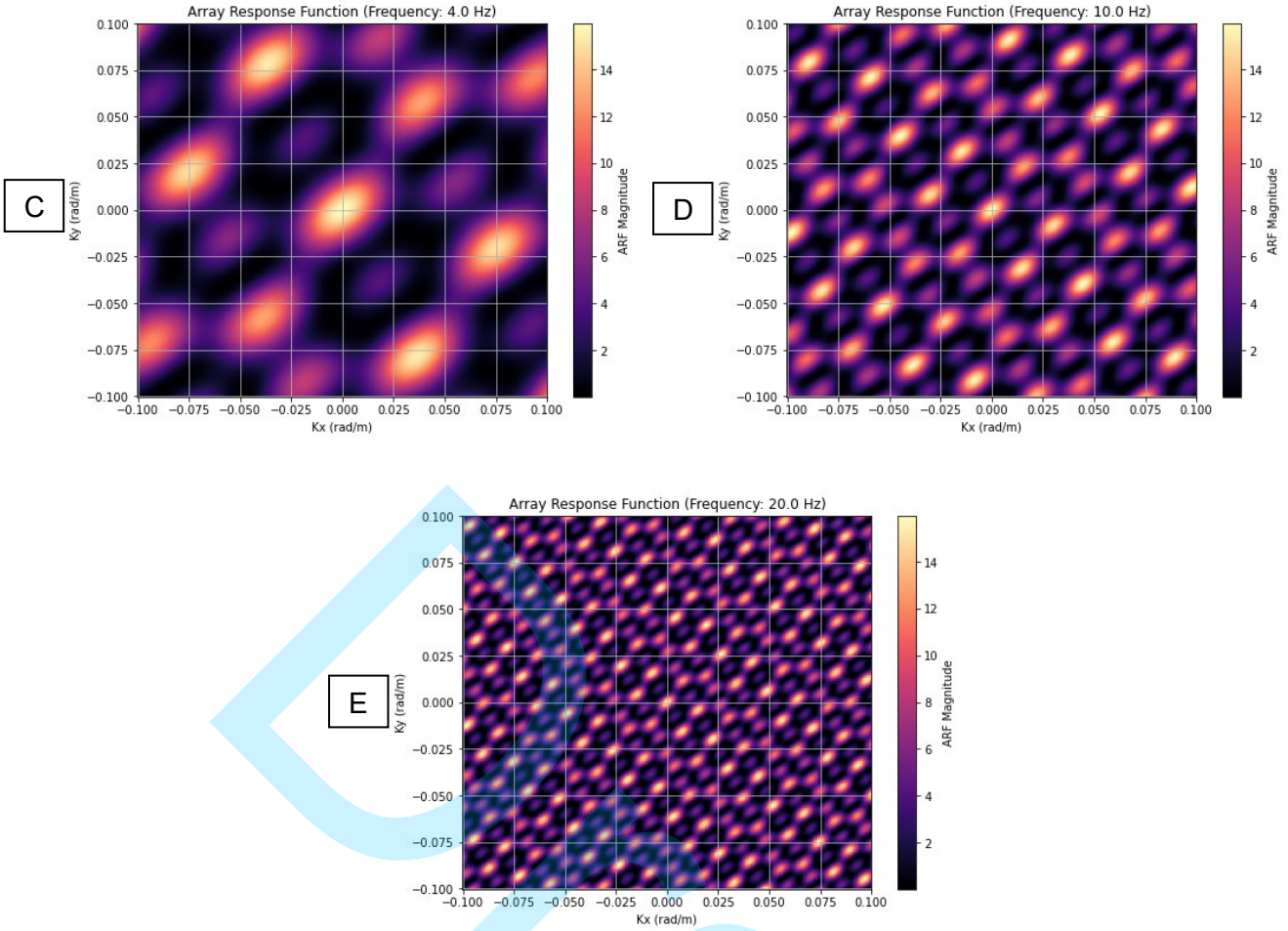


**Figure 9 –** Array responses, as a function of the wavenumbers (K in rad/m) and azimuth, relative to the propagation of the plane wavefront at a speed of 340 m/s, with frequencies from 0.1 to 20 Hz, detected by the array of IS09 station, with four elements. A) 0.1 Hz; B) 1.0 Hz; C) 4.0 Hz; D) 10 Hz; and E) 20 Hz.

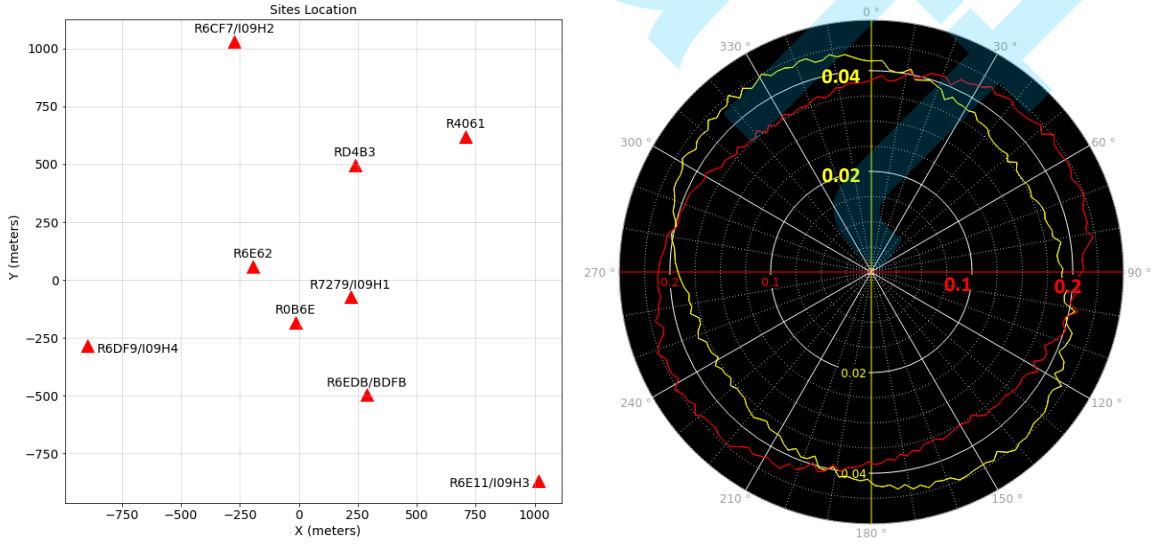


**Figure 10 –** On the left, the nine-element array proposed and, on the right, the respective polar graph of the estimated signal speed errors (red line – m/s) and azimuth (yellow line – degrees) for plane wavefronts propagating at 340 m/s. The signal sampling rate is 20 sps.

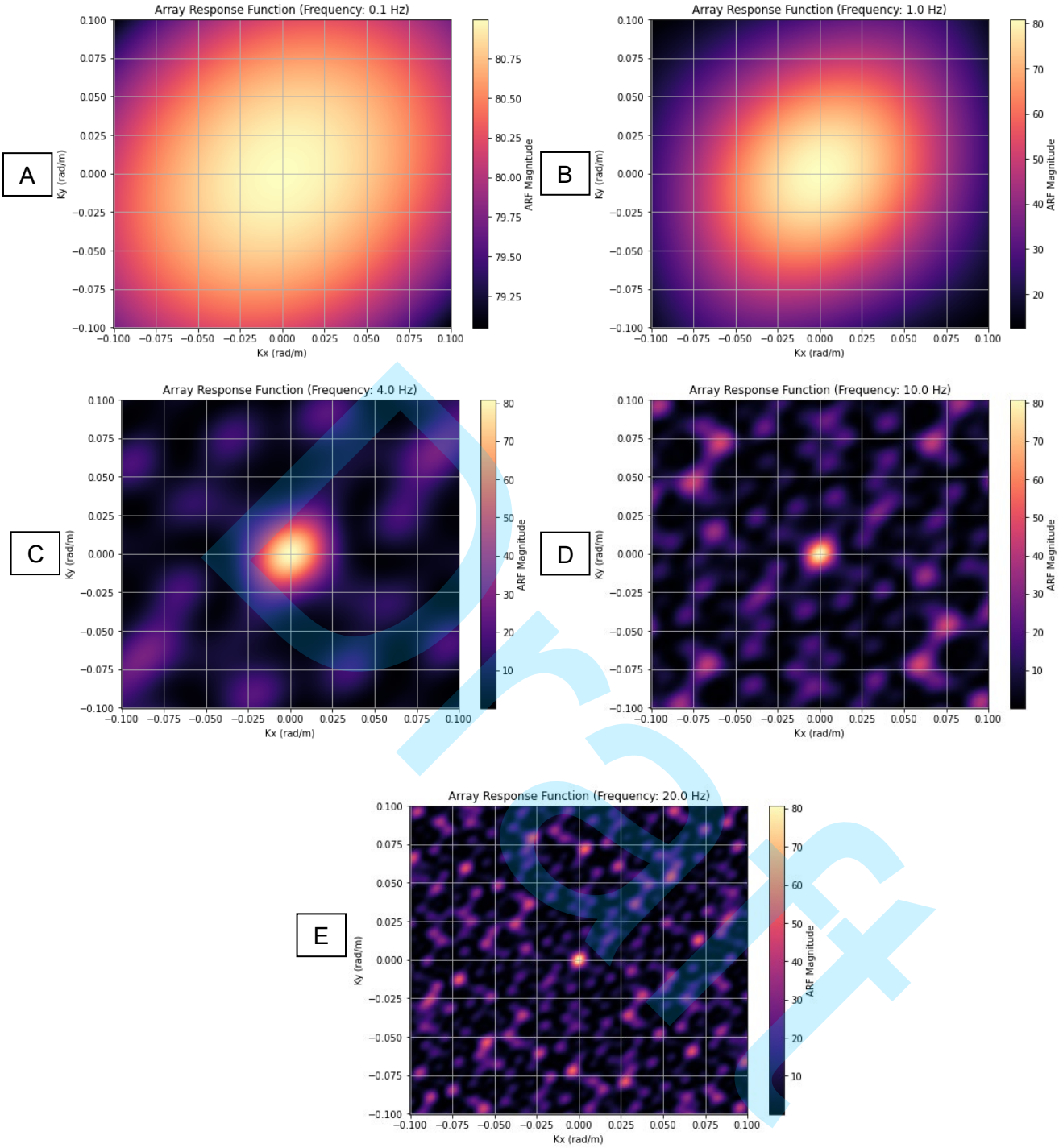


**Figure 11 –** Array responses, as a function of wavenumbers (K in rad/m) and azimuth, relative to the propagation of the plane wavefront, at a speed of 340 m/s, with frequencies from 0.1 to 20 Hz, detected by the proposed nine-element array. A) 0.1 Hz; B) 1.0 Hz; C) 4.0 Hz; D) 10 Hz; and E) 20 Hz.

***Power Spectral Density (PSD) for elements using RS&Boom and for elements with original IMS equipment***

Below, the Power Spectral Density (PSD) responses to the equipment installed at the nine points (temporary elements) in the PNB are presented, along with the PSD of the original equipment installed in the elements of the IS09 station (Fig. 12) on 02/06/2023, covering a 24-hour recording

period. It is noticeable that in “A,” the background noise level is higher than in “B.” This discrepancy in noise levels can be attributed to the superior efficiency of the mechanical filter employed in the elements of the IS09 station (with the WNRS), Marty (2019), which significantly outperforms the filter used in the temporary elements (with the Polyurethane foam and gravel). It is more evident when observing the background noise of the four temporary elements (R7279, R6CF7, R6E11, and R6DF9) situated at the same locations as the IS09 array. Additionally, the higher quality of the IS09 equipment contributes to this noise reduction (Nief et al., 2019; Marty, 2019). Nevertheless, the noise level remains acceptable, only slightly exceeding the NLNM by a few Pascals.

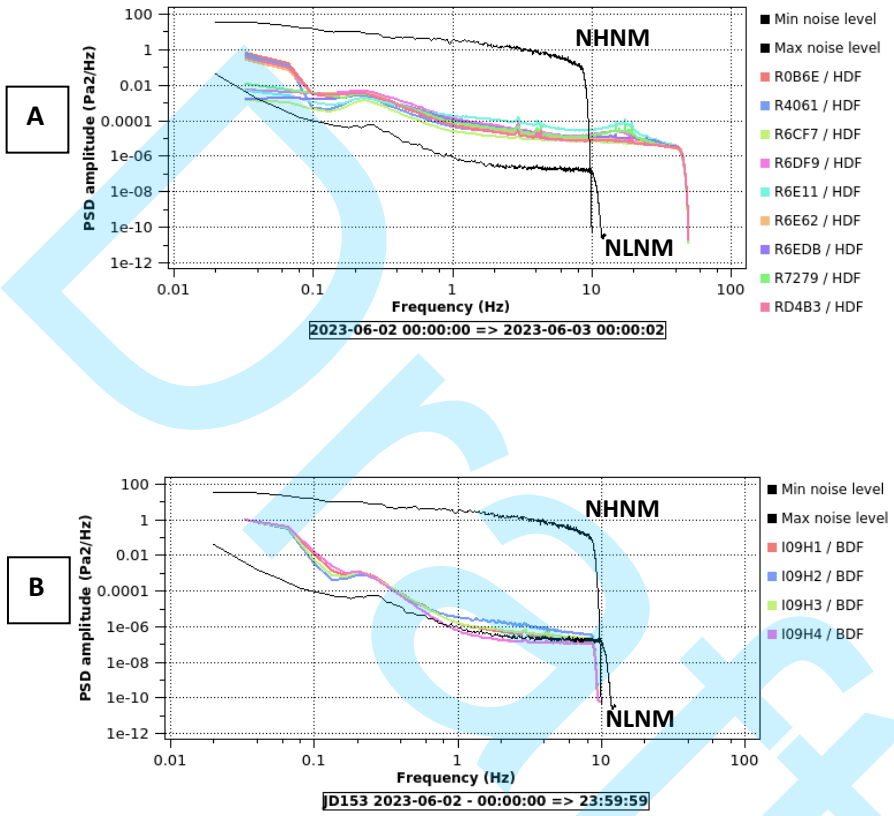


**Figure** 12 - Diagram A displays temporary elements' Power Spectral Density (PSD) using RS&Boom equipment. Diagram B shows the PSD of IS09 station elements using the original IMS equipment. Notably, in the diagram A, the equipment's frequency range surpasses that of the NHNM and NLNM curves depicted in the graph. This extension is attributed to the equipment's response capability, reaching up to 44 Hz, and the digitizer sample rate of 100 sps, in contrast to the IS09 setup configuration of 20 sps in diagram B.

***Comparison of detections based on arrays configurations***

Figures 13 to 15 depict the records and corresponding detections captured on June 2, 2023, at PNB using the nine-element array (using RS&Boom equipment) and the four-element subarray (using RS&Boom equipment and also using IMS equipment). Figure 16 presents the cumulative number of detections recorded by the nine-element array and also by the four-element array with the specific equipment type throughout their 40 days of operation (from May 19 to June 27, 2023).

**Day # 153 (06/02/2023) – 9-element array using RS&Boom equipment**

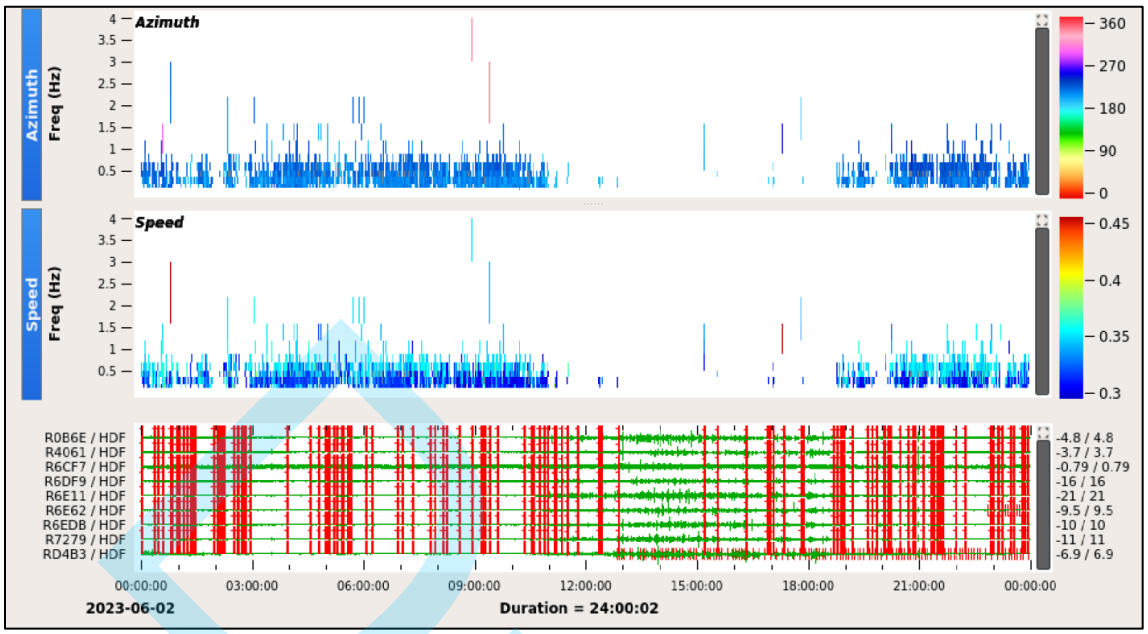


A

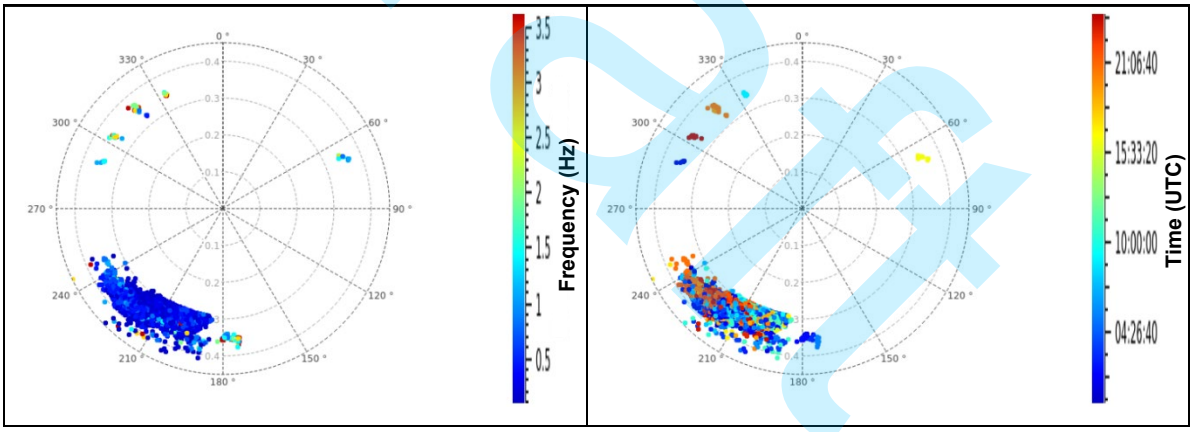


B C

**Figure 13 –** Detections from the processed signals for 24 hours of recording on 02/06/2023 at the nine temporary elements (elements). **Diagram A**, Upper Window: azimuth and frequency; Intermediate Window: frequency and speed; Lower Window: traces of infrasonic signals in the time domain. **Diagram B**, polar graph relating to frequency and speed versus azimuth of the detections recorded. **Diagram C**, polar graph relating to time and speed versus azimuth of the detections recorded.

**Day # 153 (06/02/2023) – 4-element subarray using RS&Boom equipment**

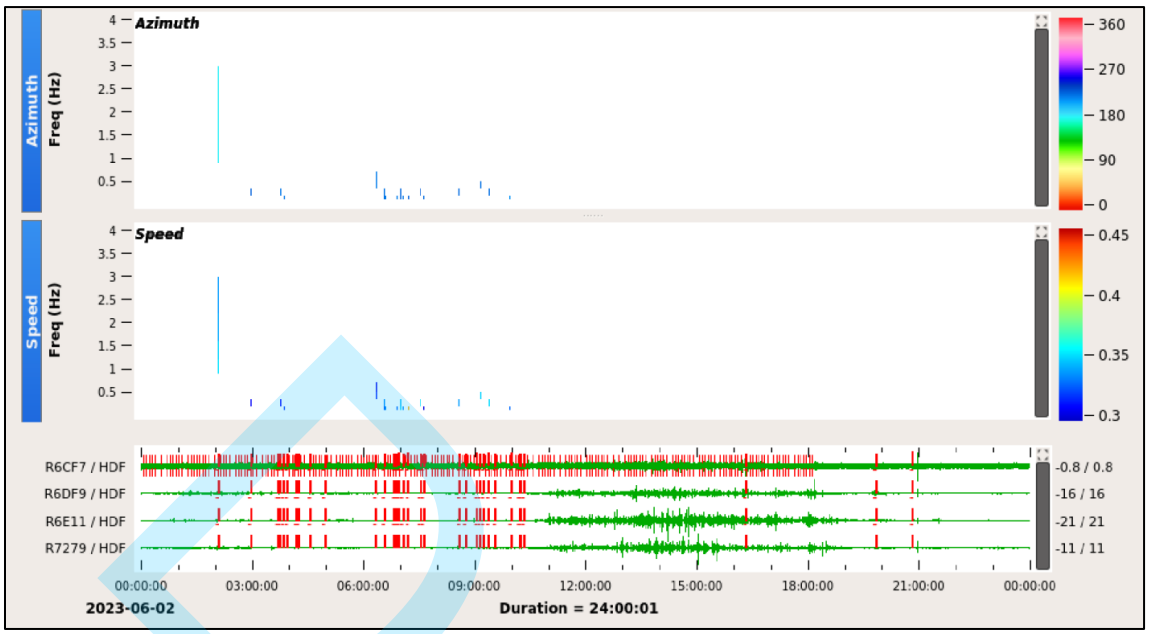


A

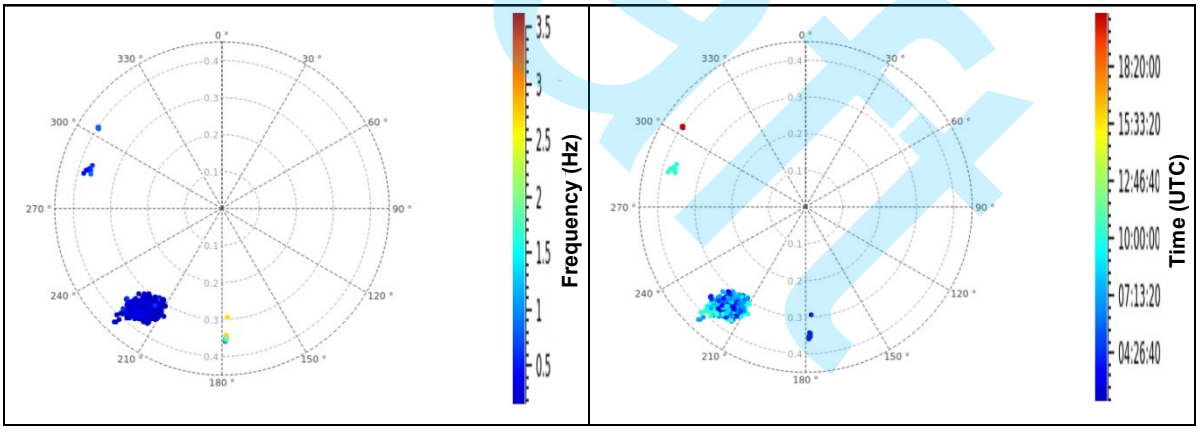


B C

**Figure 14 –** Detections from the processed signals for 24 hours of recording on 02/06/2023 at the four temporary elements. **Diagram A**, Upper Window: azimuth and frequency; Intermediate Window: frequency and speed; Lower Window: traces of infrasonic signals in the time domain. **Diagram B**, polar graph relating to frequency and speed versus azimuth of the detections recorded. **Diagram C**, polar graph relating to time and speed versus azimuth of the detections recorded.

**Day # 153 (06/02/2023) – four-element subarray using IMS equipment**

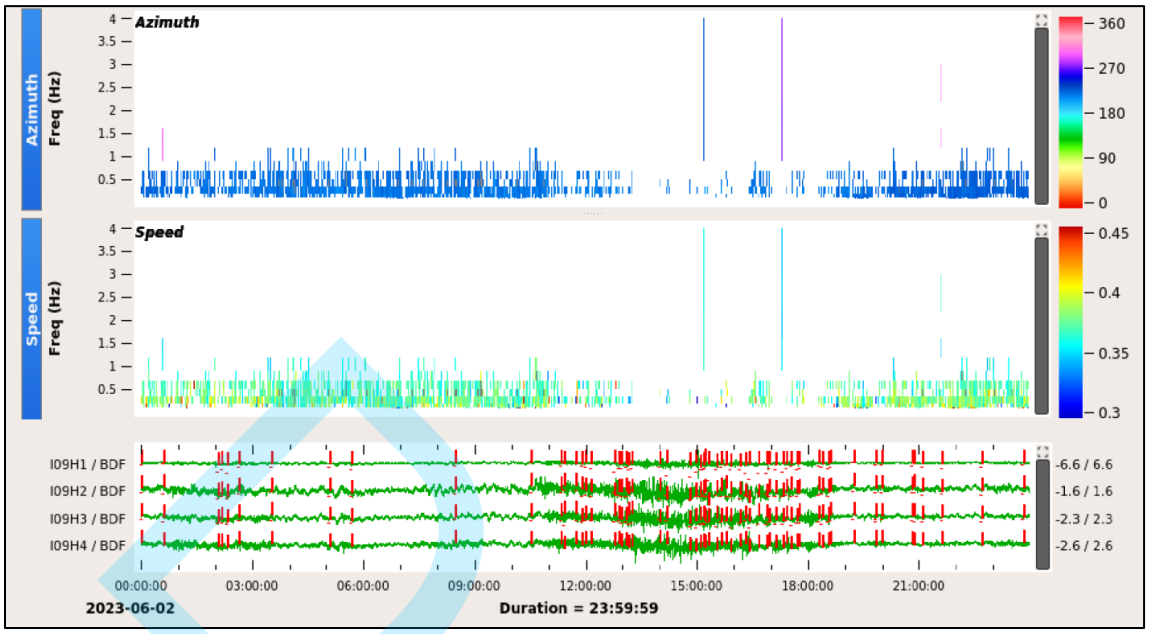


A

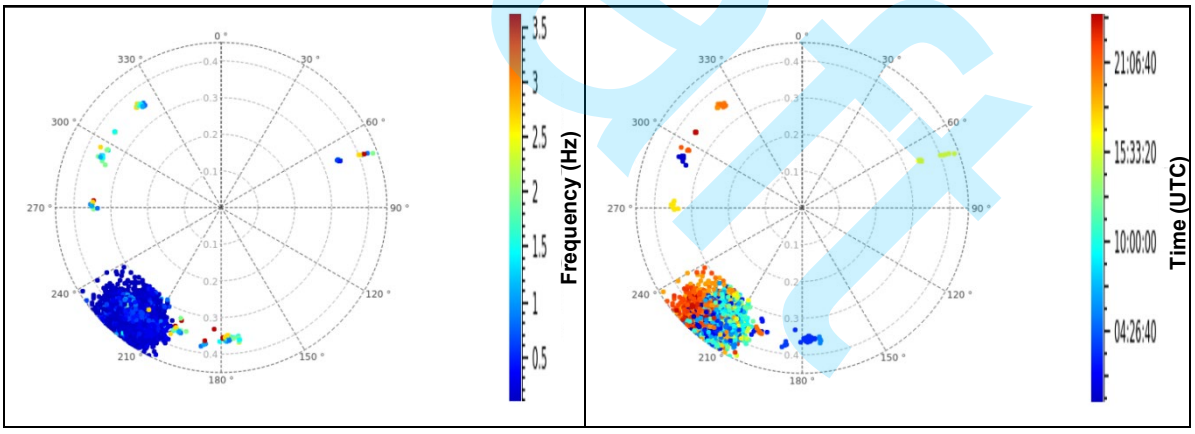


B C

**Figure 15 –** Detections from the processed signals for 24 hours of recording on 02/06/2023 at the four IMS elements (IS09). **Diagram A**, Upper Window: azimuth and frequency; Intermediate Window: frequency and speed; Lower Window: traces of infrasonic signals in the time domain. **Diagram B**, polar graph relating to frequency and speed versus azimuth of the detections recorded. **Diagram C**, polar graph relating to time and speed versus azimuth of the detections recorded.

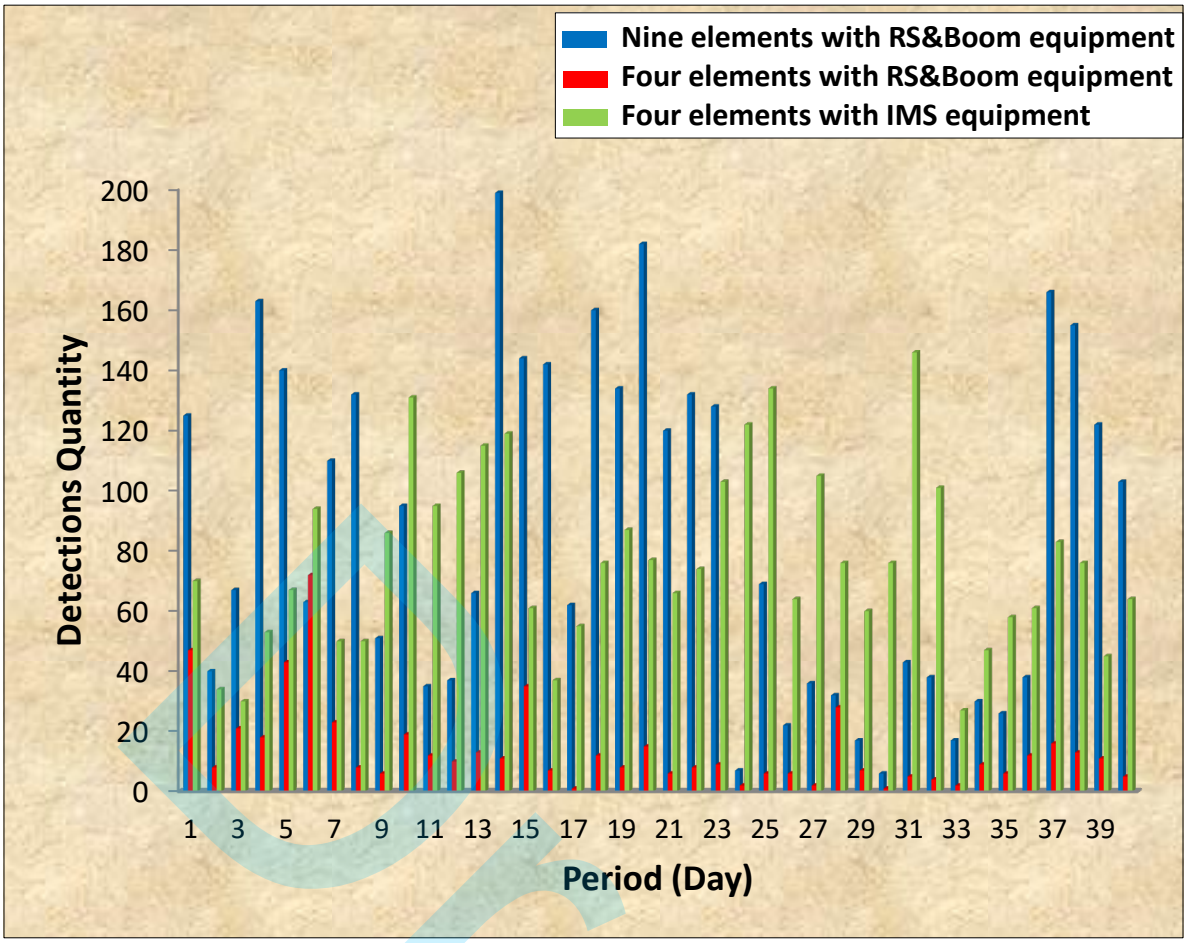


**Figure 16 –** Comparative data for the number of detections conducted by the nine-element array and four-element subarray with RS&Boom equipment and by the four-element array (IS09) with IMS equipment.

## DISCUSSION

Below (Fig. 17-A) are observed records in IS09 records in IS09 Infrasound detections relating to six days of data (October 1–6, 2018). It is observed that the highest amplitude signals are noise caused by the winds (I09 BDF channels), as they coincide with the records of the wind speed sensor installed in the I09H1 element (upper channel: I09H1/LWS). In Fig. 17-B, one day of data is detailed. The peak of the record that occurred on 10/03/2018, at 18:49 UTC, can be seen more clearly. Wind-related noise is more predominant and intense during daylight hours. Given this noise pattern, it is inferred that such occurrences are common throughout the year at the IS09 station, reflecting normal meteorological behavior. According to Campus and Christie (2010), sensors situated in high latitudes may encounter significant wind noise at any given time, whereas those in desert regions often experience pronounced wind noise during the daytime. However, neither of these scenarios reflects the conditions at the IS09 location, which is situated at a low latitude within a savannah biome.

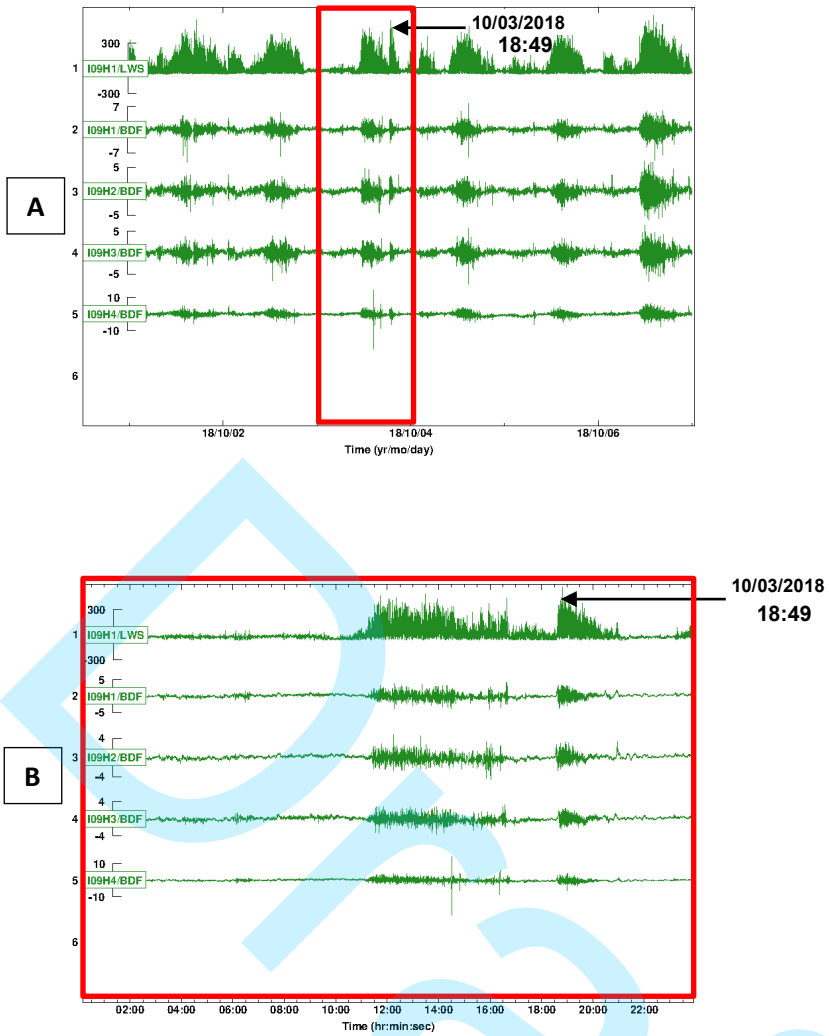


**Figure 17 –** Records, in A, corresponding to the wind speed channel (LWS) – trace 1, meteorological station installed at I09H1 element – and the infrasound signal channels (BDF), traces 2 to 5, from IS09 Station, referring to six days of data (October 1–6, 2018). In B, detail corresponds to a data day (10/03/2018). The recorded noises' correlation is observed as a function of the wind present in the IS09 elements.

We also present the data processing of the proposed nine-element array (Fig. 18) and the IS09 array (Fig. 19) using DTK-GPMCC. Both arrays recorded the same event (likely a mine explosion near PNB, approximately 20 km away) on June 2, 2023, at 16:18 UTC. The noticeable differences in the results highlight the increased accuracy of the nine-element array, which outperforms the four-element array. To improve signal clarity, a third-order Butterworth filter with a frequency range of 1-3 Hz was applied to both datasets.

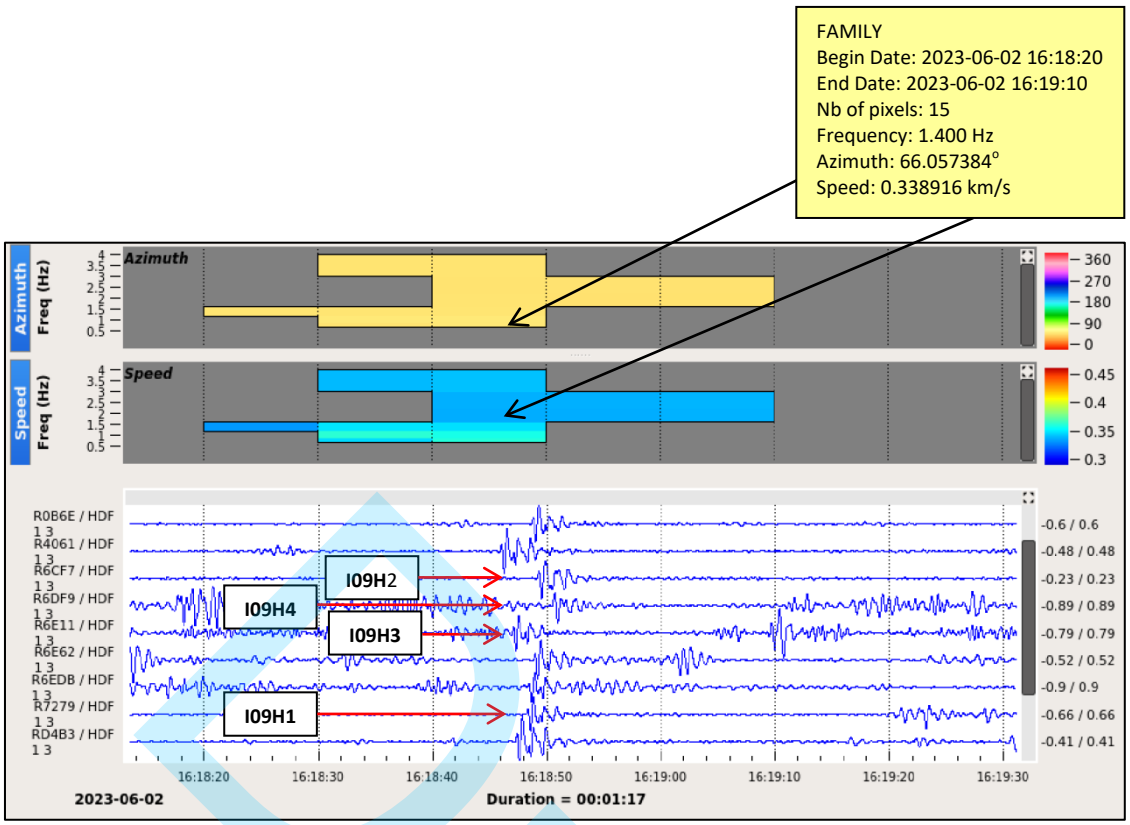


**Figure 18 –** Probable explosion on June 2, 2023, at 16:18 UTC, recorded in the nine elements of the proposed array (blue traces). The corresponding responses are displayed in the upper windows (Speed/Freq and Azimuth/Freq). The four codes associated with the records represent the temporary elements that shared sites with the IMS IS09 station elements: R6CF7 = I09H2, R6DF9 = I09H4, R6E11 = I09H3, and R7279 = I09H1. The numerical details of the obtained responses are presented in the upper yellow box.

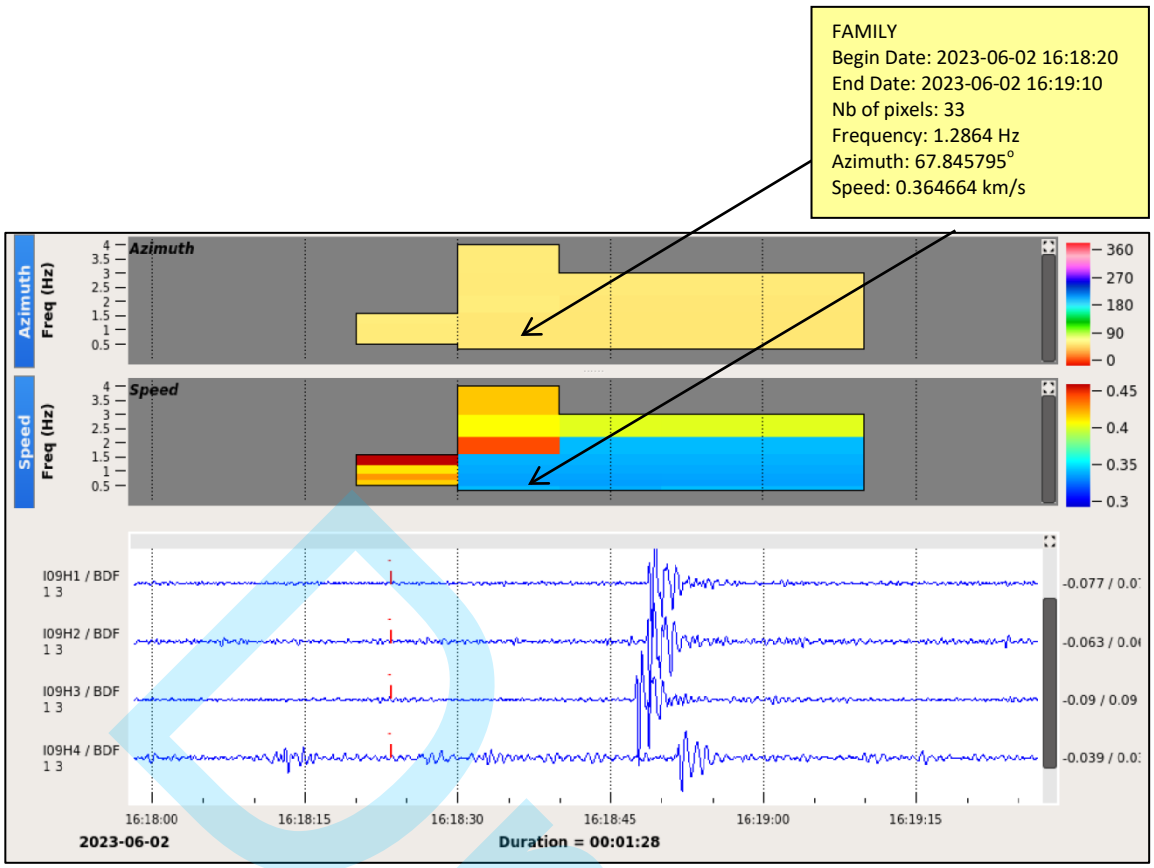


**Figure 19 –** Probable explosion on June 2, 2023, at 16:18 UTC, recorded in the four elements of the IS09 array (blue traces). The corresponding responses are displayed in the upper windows (Speed/Freq and Azimuth/Freq). The numerical details of the obtained responses are presented in the upper yellow box.

## CONCLUSIONS

The addition of five elements to the IS09's four-element array proposed in this study demonstrates a significant enhancement in detection capability compared to the former array. This improvement is substantiated through a comparative analysis between the results of the nine-element array and the four-element subarray deployed at the IS09 sites, all using the same equipment (RS&Boom). Despite the lower sensitivity of the equipment used in the nine temporary elements compared to the original IS09 elements, the data reveals a substantial increase in detections achieved by the nine-element array. The results obtained in this study are consistent with Christie (2007).

Moreover, a comparative analysis was conducted with the results obtained from the temporary subarray of four elements using RS&Boom, which shared the IS09 sites, in contrast to the IS09 results during the same period. This investigation revealed a notable difference in the number of detections, with IS09 (using IMS equipment) recording a significantly higher number. This variation can be attributed to the efficacy of the mechanical filter (using the WNRS) and the superior quality of the IMS equipment employed at IS09. Adopting the same filter and equipment used by IMS in the new elements will likely lead to an even more substantial increase in detections with this new array configuration.

The mechanical filter developed for this study (polyurethane foam with gravel covering) effectively reduced the background noise level in the elements with RS&Boom equipment, consequently improving the ability to detect small events otherwise masked by noise.

Despite the application of the filter, both in cases involving the IMS filter and the temporary elements filter developed in this study, noise is primarily recorded during daylight time when the wind is more intense. This noise compromises the array's detection capacity by masking low-amplitude coherent signals. Furthermore, the low density of trees in the savannah vegetation does not contribute to attenuating the winds over the array elements.

By directly observing the maximum value reached in the Array Response Function (ARF) of the nine-element array and of the four-element subarray, both using RS&Boom equipment, it is evident that the gain (sensitivity) relative to the nine-element array is five times greater than the gain relative to the four-element subarray. Additionally, there is a tenfold reduction in estimated uncertainties related to trace velocity and azimuth for the 9-element array.

The quality of the array equipment and the mechanical filter significantly influences the accuracy of the results obtained from data processing. Enhancing the IS09 array's response, adopting the proposed nine-element array in this study will amplify the detection capacity of the unique IMS Brazilian infrasound station. This improvement, in turn, will broaden the spectrum of recorded events, extending the scope of research beyond the objectives outlined in the Comprehensive Nuclear-Test-Ban Treaty (CTBT), which focuses on monitoring clandestine nuclear tests. Detecting events from potential new sources, will be the focus of future studies.

## REFERENCES

Alcoverro, B. and A. Le Pichon, 2005, Design and optimization of a noise reduction system for infrasonic measurements using elements with low acoustic impedance. J Acoust Soc Am 117(4):1717–1727. DOI: 10.1121/1.1804966.

Alcoverro, B., 1998, Acoustic filters design and experimental results. Proceedings Workshop on Infrasound. DASE, Commissariat à l'Energie, Bruyères-le-Châtel, France.

Barros, L., B. Neri, J. Carvalho and D. Fontenele, 2020, Brazilian participation in the verification of the Comprehensive Nuclear-Test-Ban Treaty. Tubarão (SC): Copiart, 2020. 152p.

Barros, L. and D. Fontenele, 2002, IS09 Infrasound Station – International Monitoring System, FINAL REPORT Site Preparation, Construction and Installation, Seismological Observatory of the University of Brasília, Brazil. September 2002, 254 p.

Bass, H. E. and F. D. Shields, 2004, The use of arrays of electronic sensors to separate infrasound from wind noise, in Proceedings of the 26th Seismic Research Review: Trends in Nuclear Explosion Monitoring, LA-UR-04-5801, Vol. 1, pp. 601–607.

Beyreuther, M., R. Barsch, L. Krischer, T. Megies, Y. Behr and J. Wassermann, 2010, ObsPy: a Python toolbox for seismology, Seismol. Res. Lett., 81(3), 530–533. DOI: 10.1785/gssrl.81.3.530.

Bishop, J. W., D. Fee and C. A. L. Szuberla, 2020, Improved infrasound array processing with robust estimators. Geophys. J. Int. 221, 2058–2074 DOI: 10.1093/gji/ggaa110.

Bowman, J.R., G. E. Baker and M. Bahavar, 2005, Ambient infrasound noise, Geophys. Res. Lett., 32(9), L09803. DOI: 10.1029/2005GL022486.

Brachet, N., D. Brown, R. Le Bras, Y. Cansi, P. Mialle and J. Coyne, 2010, Monitoring the Earth's atmosphere with the global IMS infrasound network. In: Le Pichon, A., Blanc, E., Hauchecorne, A. (eds) Infrasound Monitoring for Atmospheric Studies. Springer, Dordrecht. p. 77-118. DOI: 10.1007/978-1-4020-9508-5_3.

Campus, P. and D. Christie, 2010, Worldwide observations of infrasonic waves. In: Le Pichon A, Blanc E., Hauchecorne A. (eds) Infrasound monitoring for atmospheric studies. Springer, Berlin, Germain, pp 29–75. DOI: 10.1007/978-1-4020-9508-5_6.

Cansi, Y.,1995, An automatic seismic event processing for detection and location: The P.M.C.C. method. Geophysical Research Letters, 22(9), 1021–1024. https://doi.org/10.1029/95GL00468.

CEA/DASE, 2016a, DKT-GPMCC – User Manual. Dase ToolKit - Graphical Progressive Multi-Channel Correlation (DTK-GPMCC). Commissariat à L'énergie Atomique et Aux Énergies Alternatives (CEA).

Christie, D., B. L. N. Kennett and C. Tarlowski, 2007, Advances in infrasound technology with application to nuclear explosion monitoring. 29th Monitoring Research Review: Ground-Based Nuclear Explosion Monitoring Technologies. Australian National University. Sponsored by Air Force Research Laboratory Contract No.: FA8718-04-C-0032.

CTBTO, 1997, Report of working group B to the second session of the preparatory commission for the Comprehensive Nuclear-Test-Ban Treaty Organization, Annex 2 (CTBT/PC/II/1/Add.2), Vienna. Available on: <https://digitallibrary.un.org/record/240417>.

CTBTO, 2001, Report of working group B to the fifteen session of the Preparatory Commission for the Comprehensive Nuclear-Test-Ban Treaty Organization, (CTBT/PC-37/WGB/1), Vienna.

CTBTO, 2003, Minutes of infrasound experts meeting. Comprehensive Nuclear-Test-Ban Treaty Organization. University of California, San Diego (UCSD), La Jolla. Report of Working Group B to the second session of the Preparatory Commission for the Comprehensive Nuclear Test-Ban Treaty Organization.

CTBTO, 2009, Operational manual for infrasound monitoring and the international exchange of infrasound data – draft Comprehensive Nuclear-Test-Ban Treaty Organization, Task Leader (CTBT/WGB/TL-11,17/17/Rev.5). Vienna. (CTBT/WGB/TL-11,17/17/Rev.5).

Dahlman, O., J. Mackby, S. Mykkeltveit and H. Haak, 2011, Detect and Deter: Can Countries Verify the Nuclear Test Ban? Springer Science and Business Media - 271p. DOI: 10.1007/978-94-007-1676-6.

Green, D.N., 2015, The spatial coherence structure of infrasonic waves: analysis of data from International Monitoring System arrays, Geophys. J. Int., 201(1):377-389. DOI: 10.1093/gji/ggu495.

Green, D.N. and D. Bowers, 2010, Estimating the detection capability of the International Monitoring System infrasound network, J. geophys. Res., 115 (D18). DOI: 10.1029/2010JD014017.

Havskov, J. and G. Alguacil, 2004, Instrumentation in Earthquake Seismology. Springer, Netherlands, 358 pp. ISBN 1-4020-2968-3.

Hedlin, M.A.H. and R. Raspet, 2003, Infrasonic wind-noise reduction by barriers and spatial filters, J. Acoust. Soc. Am., 114(3), 1379–1386. DOI: 10.1121/1.1598198.

Mack, H. and E. Flinn, 1971, Analysis of the spatial coherence of short-period acoustic-gravity waves in the atmosphere. Geophys. J. Int.26:255–269. DOI: 10.1111/j.1365-246X.1971.tb03399.x.

Marty J., 2019, The IMS Network: current status and technological developments, in Infrasound Monitoring for Atmospheric Studies, 2nd ed., pp. 3–62., eds. Le Pichon A, Blanc E., Hauchecorne A., Springer, Cham. DOI: 10.1007/978-3-319-75140-5_1.

McNamara, D. E. and R. P. Buland, 2004, Ambient noise levels in the continental United States. Bulletin of the Seismological Society of America, 94(4), 1517–1527. https://doi.org/10.1785/012003001.

Nief, G., C. Talmadge, J. Rothman and T. Gabrielson, 2019, New generations of infrasound sensors: technological developments and calibration, in Infrasound Monitoring for Atmospheric Studies, 2nd ed., pp. 63–89., eds. Le Pichon A, Blanc E., Hauchecorne A., Springer, Cham. DOI: 10.1007/978-3-319-75140-5_2.

Peterson, J., 1993, Observations and Modeling of Seismic Background Noise. U.S.G.S, Open-File Report, 93-

322, 95 p. DOI: 10.3133/ofr93322.

RaspberryShake Specifications, 2022, Accessed from https://raspberryshake.org/wp-content/uploads/2020/07/Specifications-ShakeBoom.pdf, March 2023.

Ruigrok, E., S. Gibbons and K. Wapenaar, 2017, Cross-correlation beamforming. Journal of Seismology, 21, 495–508. DOI: 10.1007/s10950-016-9612-6.

Walker, K.T. and M. Hedlin, 2010, A review of wind-noise reduction methodologies, Infrasound Monitoring for Atmospheric Studies, chap. 5, vol. 1, pp. 141–182, eds Le Pichon, A., Blanc, E. and Hauchecorne, A., Springer Science+Business Media. DOI: 10.1007/978-1-4020-9508-5_5.

**Fontenele, D. P.:** research of the subject-matter (methodology), development of the mechanical filter, install the equipment in the field and collect the data, analysis of the data, write the manuscript; **Barros, L. V.:** review the entire manuscript, contributions on the methodology applied.